Supplement of Solid Earth, 13, 1455–1473, 2022
https://doi.org/10.5194/se-13-1455-2022-supplement

Solid Earth Open Access EGU

Supplement of

The effect of low-viscosity sediments on the dynamics and accretionary style of subduction margins

Adina E. Pusok et al.

Correspondence to: Adina E. Pusok (adina.pusok@earth.ox.ac.uk)

List of figures and tables:

Repository details:

The repository containing the input parameters files to reproduce the data can be found at: https://adina@bitbucket.org/adina/rep-msubdsed.git. The full simulation data ($>$ 100Gb) presented in this study can be provided on request from AP.

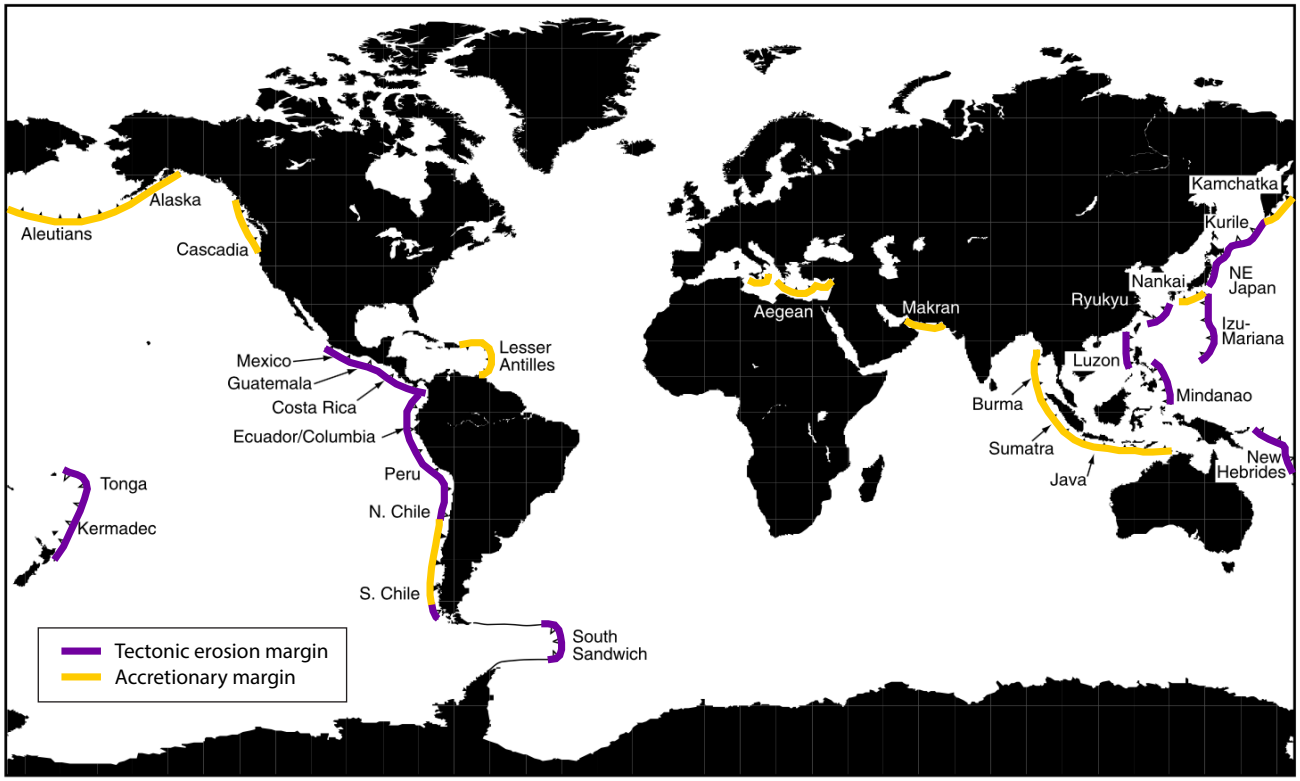

Figure S1. Global map of the subduction system modified from Clift and Vannucchi (2004) with the dominant margin type averaged for the last 10 Myrs. Colours: purple - tectonic erosion, yellow - accretionary margin.

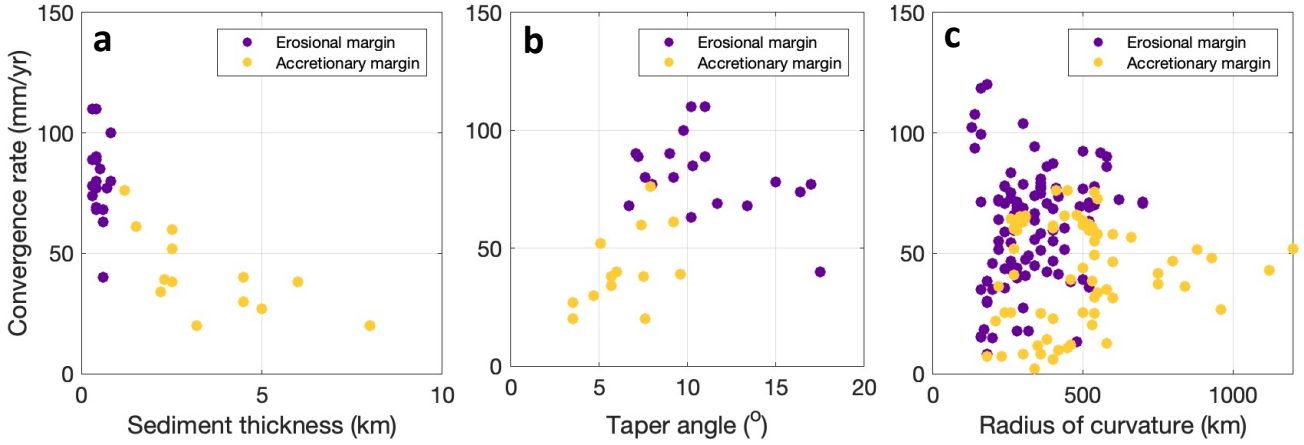

Figure S2. Replotted published data for the global subduction system. a) Convergence rate versus sediment thickness from Clift and Vannucchi (2004). Each point represents mean value for a subduction zone averaged for the last 10 Myrs. b) Convergence rate versus taper angle of accretionary wedge (low taper angle means wider accretionary wedge). Data from Clift and Vannucchi (2004) c) Convergence rate versus radius of curvature from Wu et al. (2008). The points in this plot represent present-day values for 173 segments in the subduction system (a subduction zone may be split into multiple segments). We used the margin classification from Clift and Vannucchi (2004) to color code the data for margin type. A preliminary inspection shows distinct clusters for the margin types in all plots.

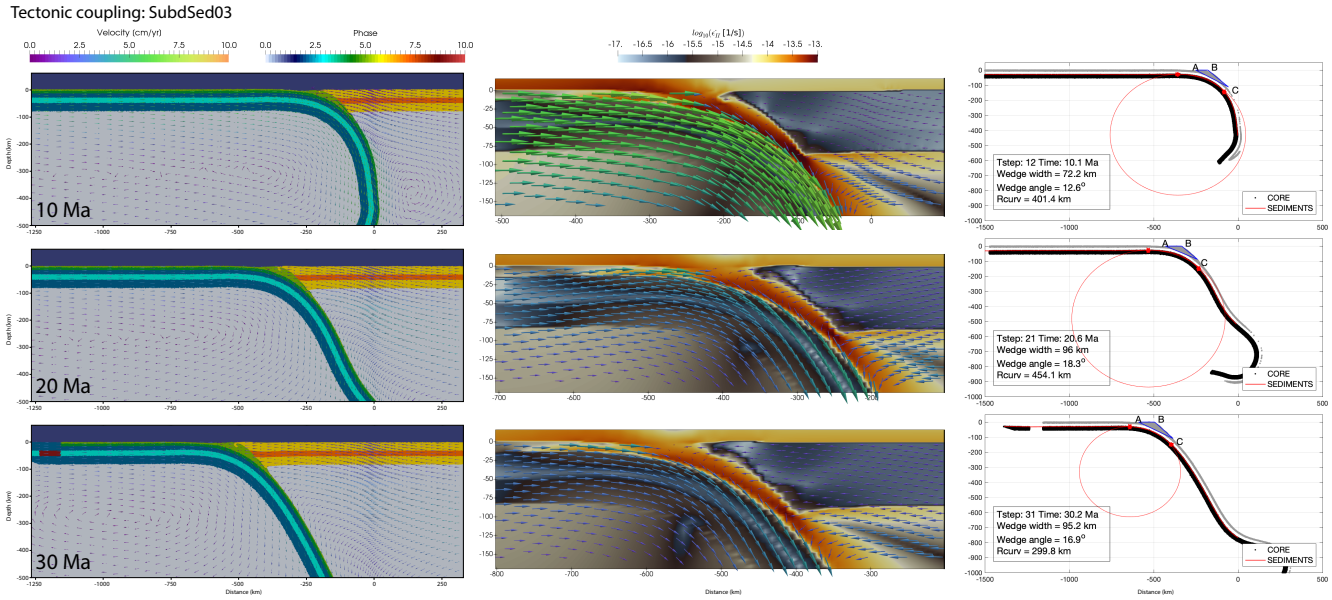

Figure S3. Tectonic coupling model (SubdSed03) shown at 10 Ma, 20 Ma and 30 Ma. Left column shows phases, middle column shows second invariant of strain rate ($\dot{\epsilon}_{II}$), and right column shows slab and wedge geometry. The interface retains a constant geometry throughout the evolution of the model.

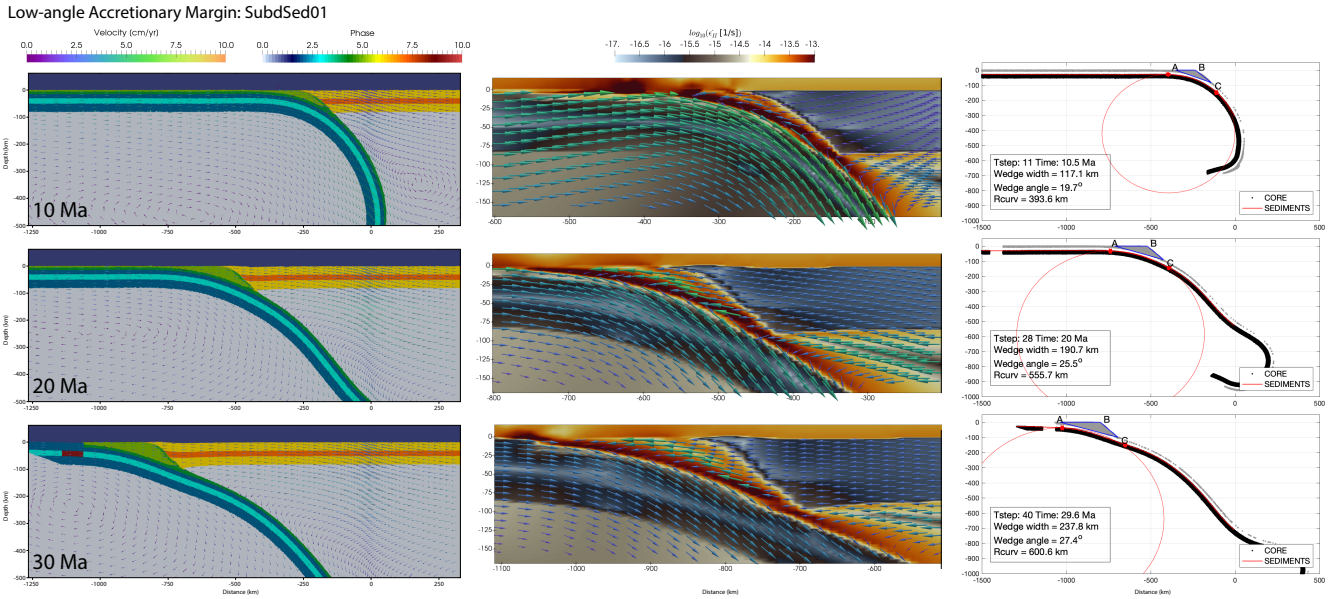

Figure S4. Low-angle accretionary margin model (SubdSed01) shown at 10 Ma, 20 Ma and 30 Ma. Left column shows phases, middle column shows second invariant of strain rate ($\dot{\epsilon}_{II}$), and right column shows slab and wedge geometry. Wedge geometry increases over time, with fast plate convergence, but which remains relatively constant. Strain-rate maps indicate that plate convergence is accommodated at the base of the accretionary wedge.

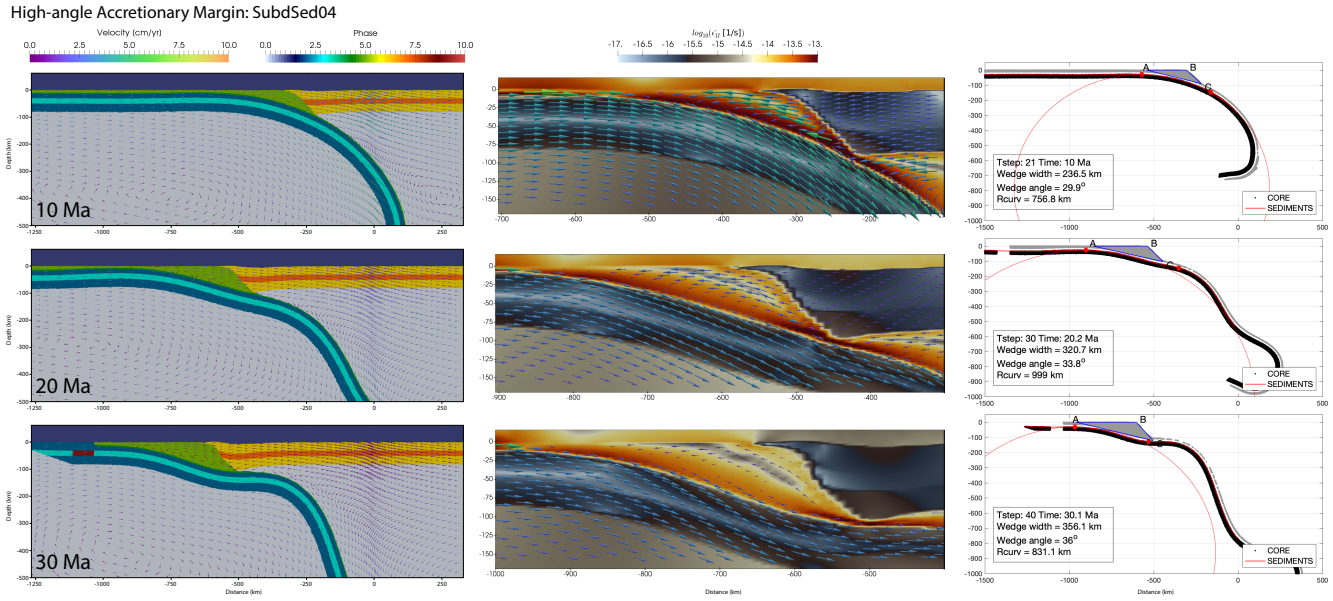

Figure S5. High-angle accretionary margin model (SubdSed04) shown at 10 Ma, 20 Ma and 30 Ma. The upper plate has a thickness of 80 km. Left column shows phases, middle column shows second invariant of strain rate ($\dot{\epsilon}_{II}$), and right column shows slab and wedge geometry. Model results at 10 Ma show a low-angle accretionary wedge, with fast convergence rate. As the wedge grows over time, it drastically changes subduction; the wedge bends the slab, leading to flat-slab subduction at 30 Ma. Convergence has slowed down considerably.

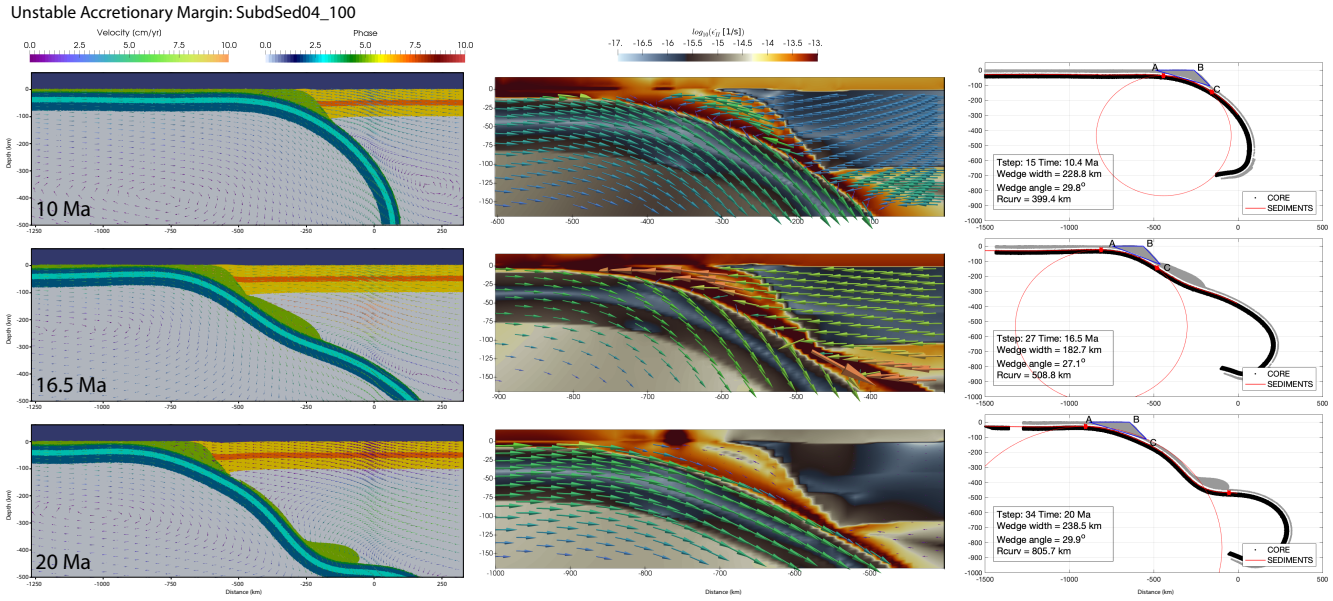

Figure S6. Unstable accretionary margin model (SubdSed04_100) shown at 10 Ma, 16.5 Ma and 20 Ma. The upper plate has a thickness of 100 km compared to SubdSed04. Left column shows phases, middle column shows second invariant of strain rate ($\dot{\epsilon}_{II}$), and right column shows slab and wedge geometry. When the wedge grows larger than a critical angle (in this case, $\sim 35^o$), the base of the upper plate deforms in order to allow piles of sediments to subduct in the mantle. After this episode, the wedge starts growing until it reaches the critical angle again. The unstable mode is overestimated in our models due to the high density of sediments.

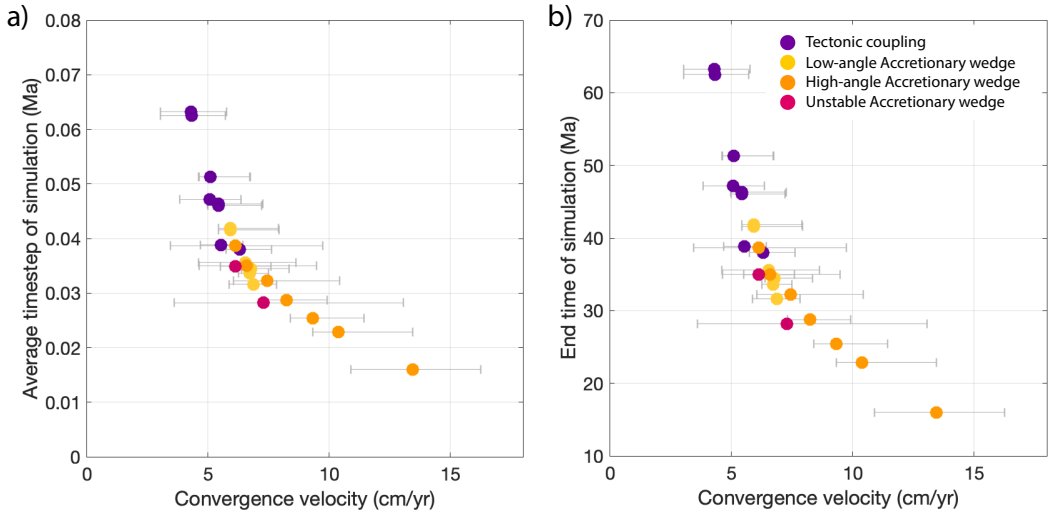

Figure S7. Simulation time (a) and timestep (b) versus convergence velocity and margin type. The plots show the dependence of timestep size on input parameters and dynamics. The timestep size is calculated using the Courant-Friedrichs-Lewy (CFL) criterion, which is a function of the maximum velocity and grid size in the model.

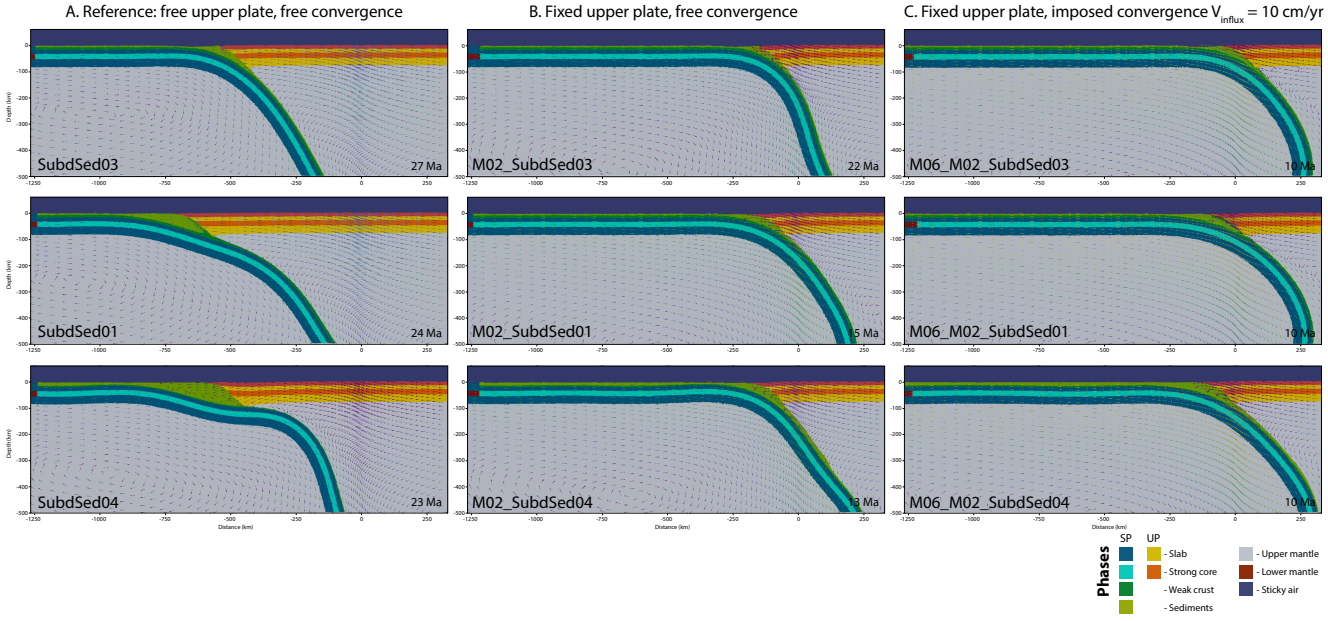

Figure S8. Reference models (SubdSed03, Subdsed01, SubdSed04) and different boundary conditions - Model snapshots after same amount of plate convergence. A. Reference models. B. Upper plate is fixed to the right wall, meaning that trench retreat is also modulated by plate deformation. Dynamics is still driven by free subduction (i.e., slab-pull). C. Imposed convergence (V_{influx} = 10 cm/yr) with a fixed upper plate. In this set of experiments, we test an opposite scenario, in which plate convergence dictates sediment behaviour.

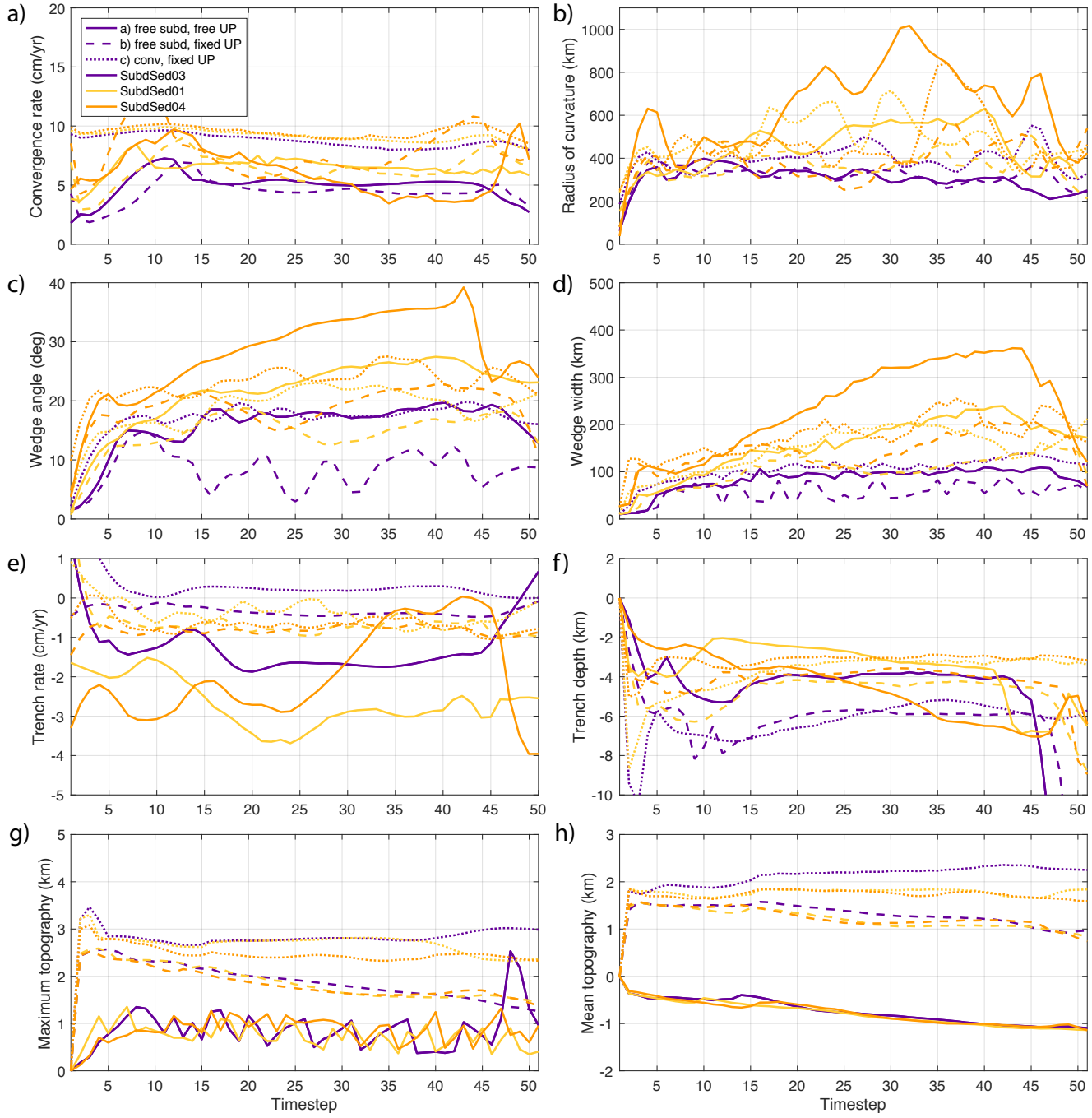

Figure S9. Reference models (SubdSed03, Subdsed01, SubdSed04) and different boundary conditions - Evolution of diagnostic parameters. Solid lines - Reference models (A), dashed lines - Upper plate is fixed to the right wall (B), dotted lines - Imposed convergence (V_{influx} = 10 cm/yr) with a fixed upper plate (C). A fixed upper plate (cases B,C) has the largest influence on topographic signals.

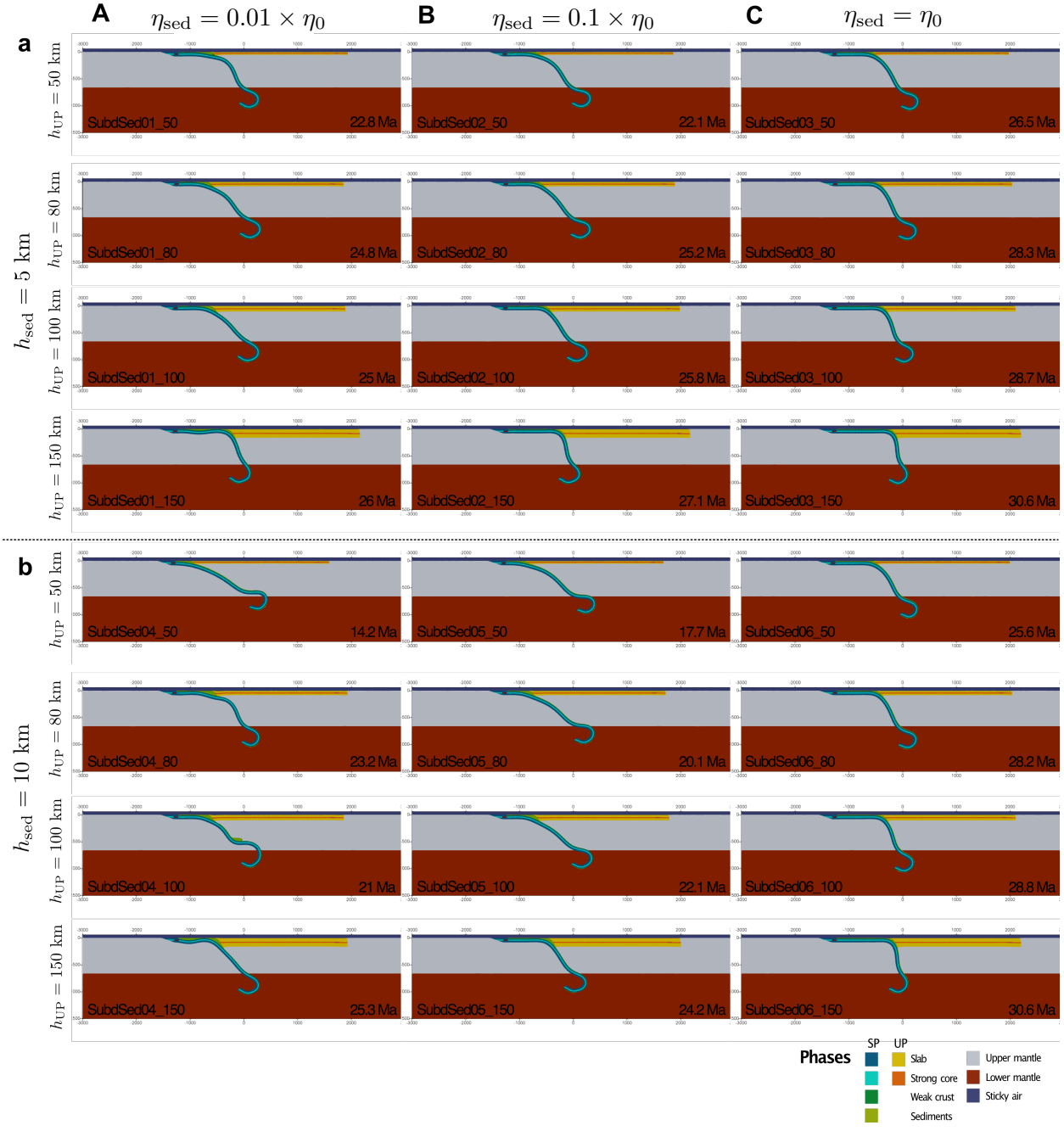

Figure S10. Simulation results at reference timestep - Whole domain phases. Columns represent simulations with different sediment viscosities (A-C), and rows represent simulations with different sediment thicknesses (a-b) and different upper plate thicknesses.

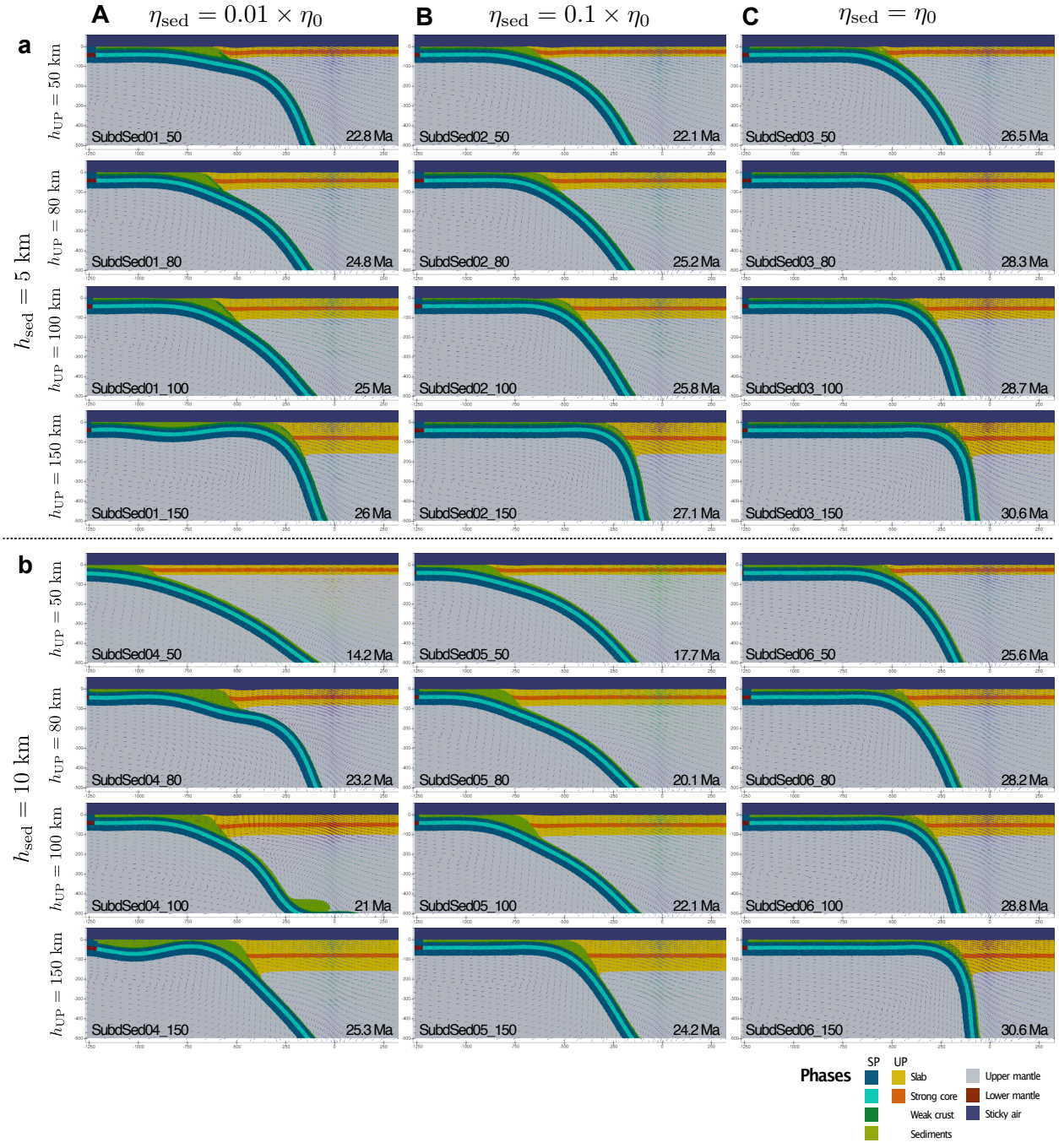

Figure S11. Simulation results at reference timestep - Zoom area phases.

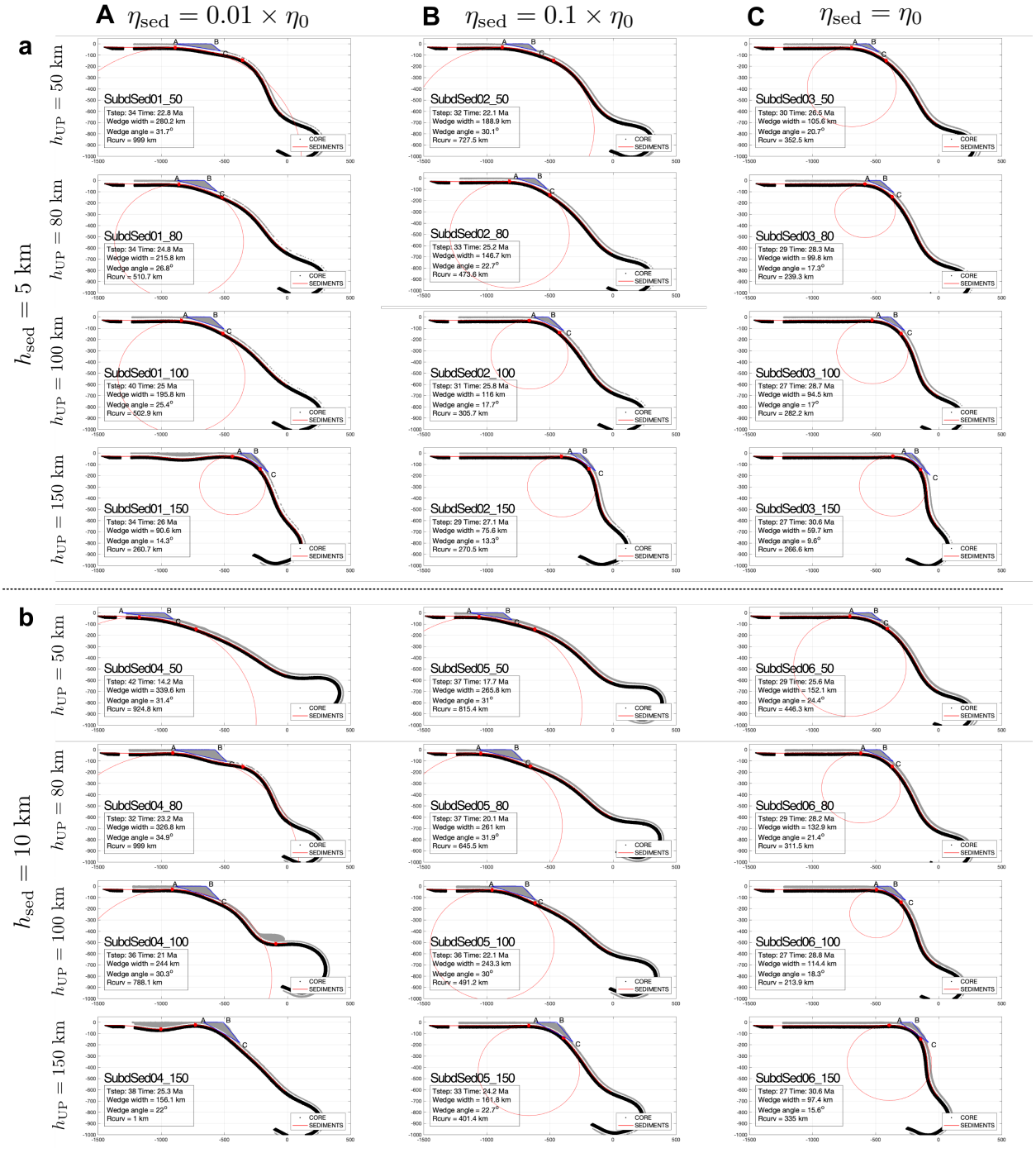

Figure S12. Simulation results at reference timestep - Calculations of radius of curvature, wedge angle and wedge width.

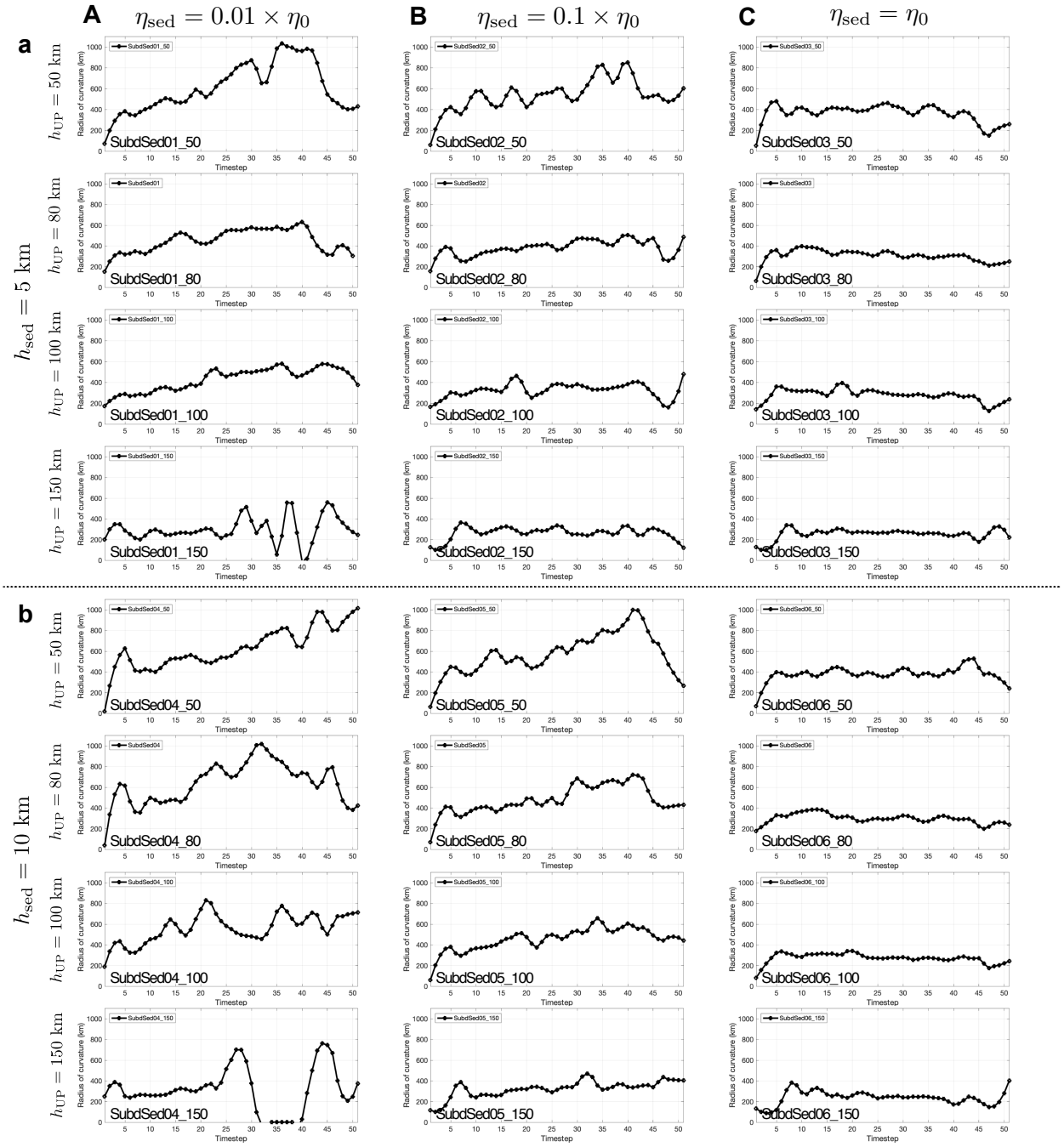

Figure S13. Simulation results - Evolution of radius of curvature. The algorithm to calculate the radius of curvature is generally robust. In cases of extreme slab bending (i.e., SubdSed04_150) when it cannot find a solution, the algorithm returns zero values.

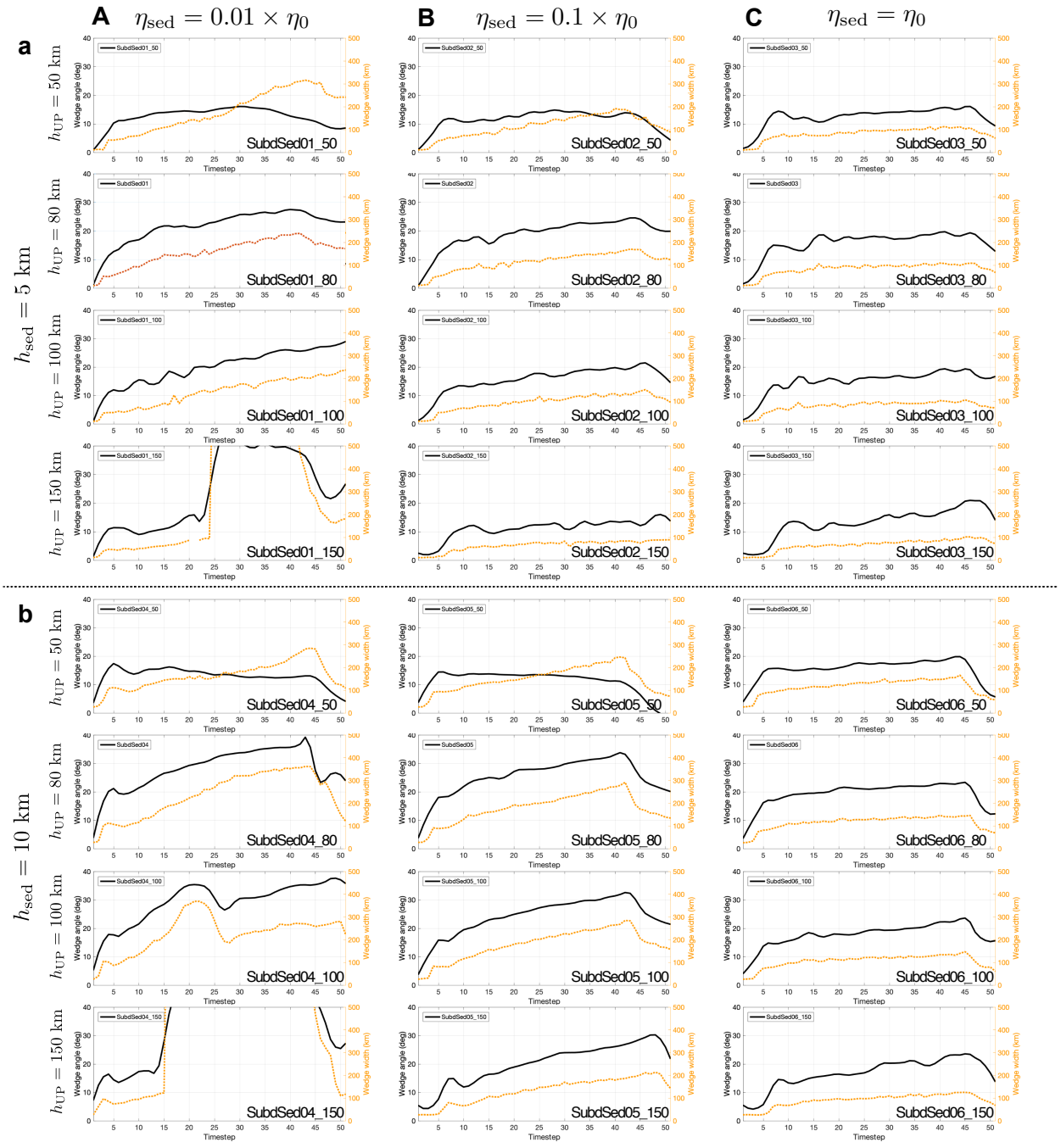

Figure S14. Simulation results - Evolution of wedge angle (black) and width (yellow). In unstable AW regimes (e.g., SubdSed01_150, SubdSed04_150), the algorithm to calculate the wedge properties also becomes less reliable because the wedge geometry changes very quickly.

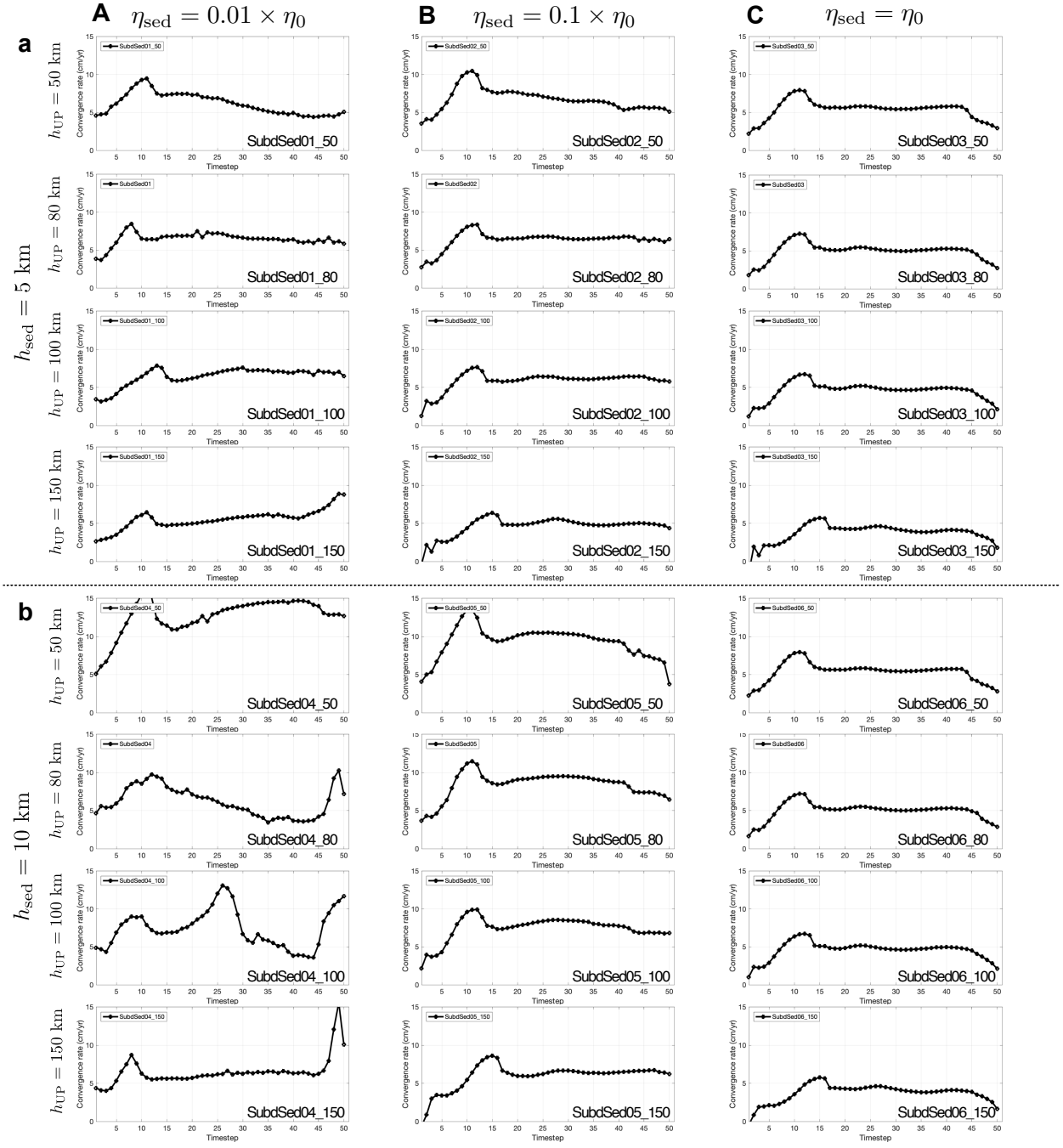

Figure S15. Simulation results - Evolution of convergence rate.

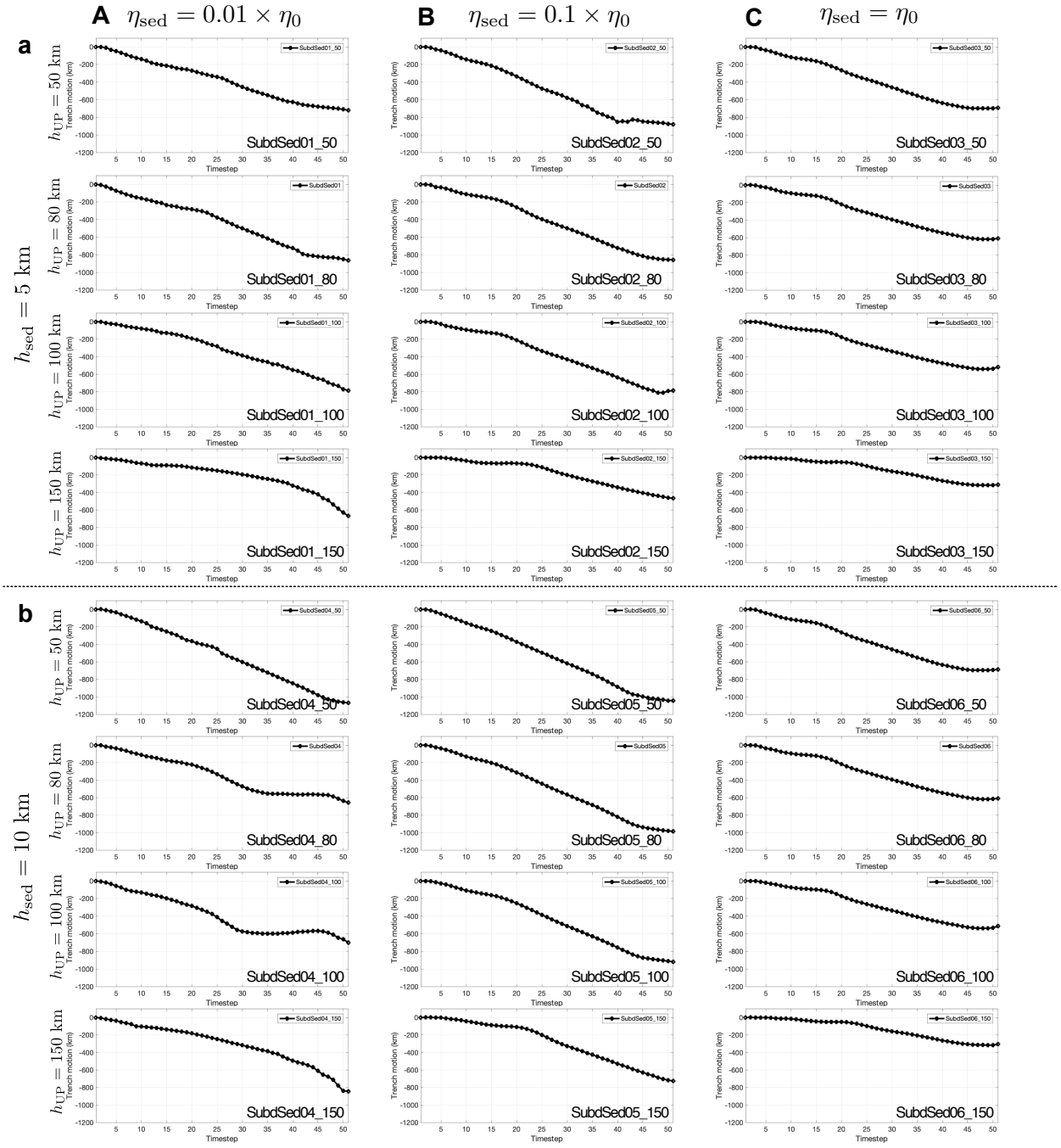

Figure S16. Simulation results - Evolution of trench position. Trench rate is calculated as $\frac{dx_T}{dt}$.

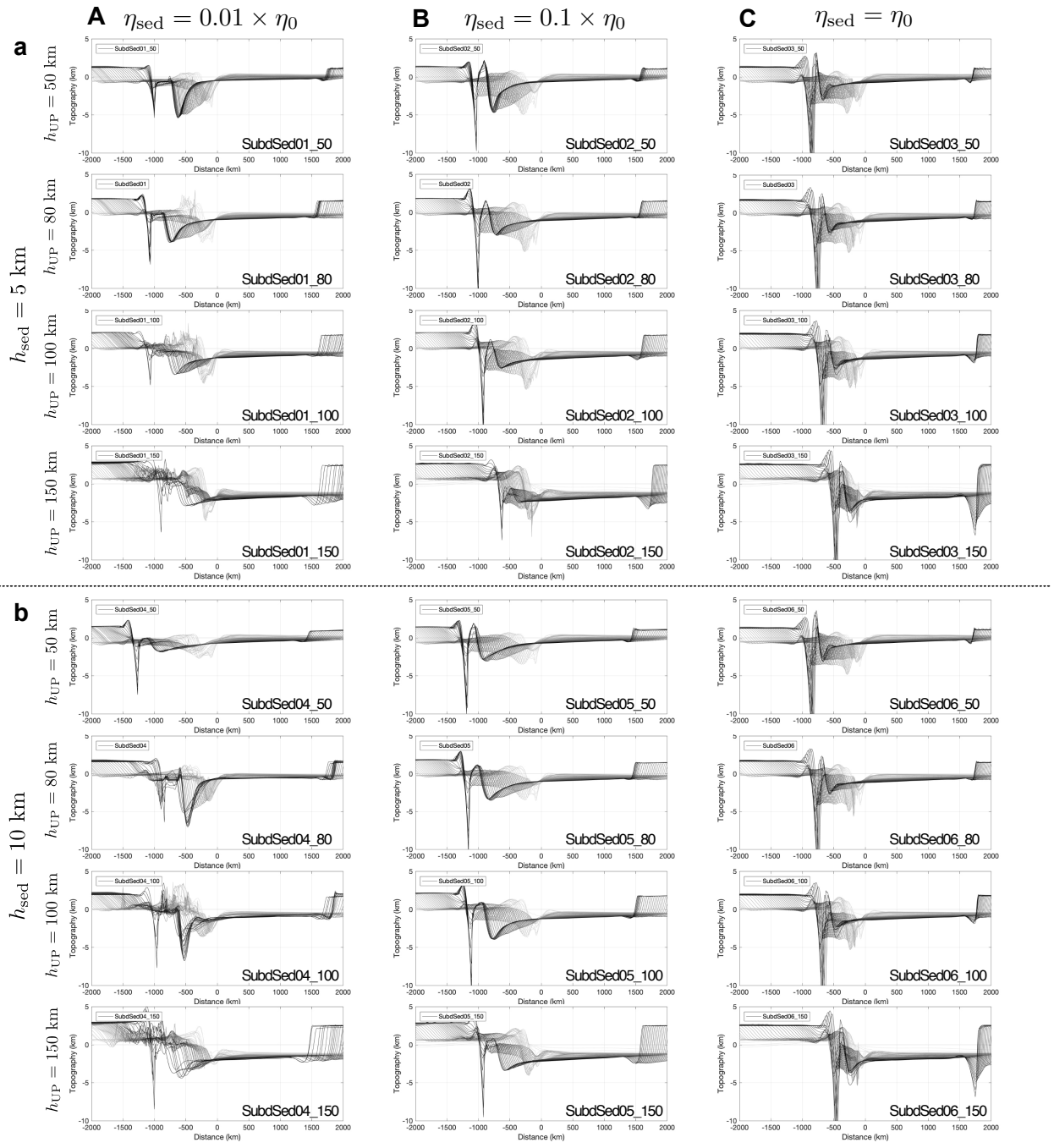

Figure S17. Simulation results - Evolution of topography. Topographic profiles at each time step are plotted from white (initial conditions) to black (final conditions).

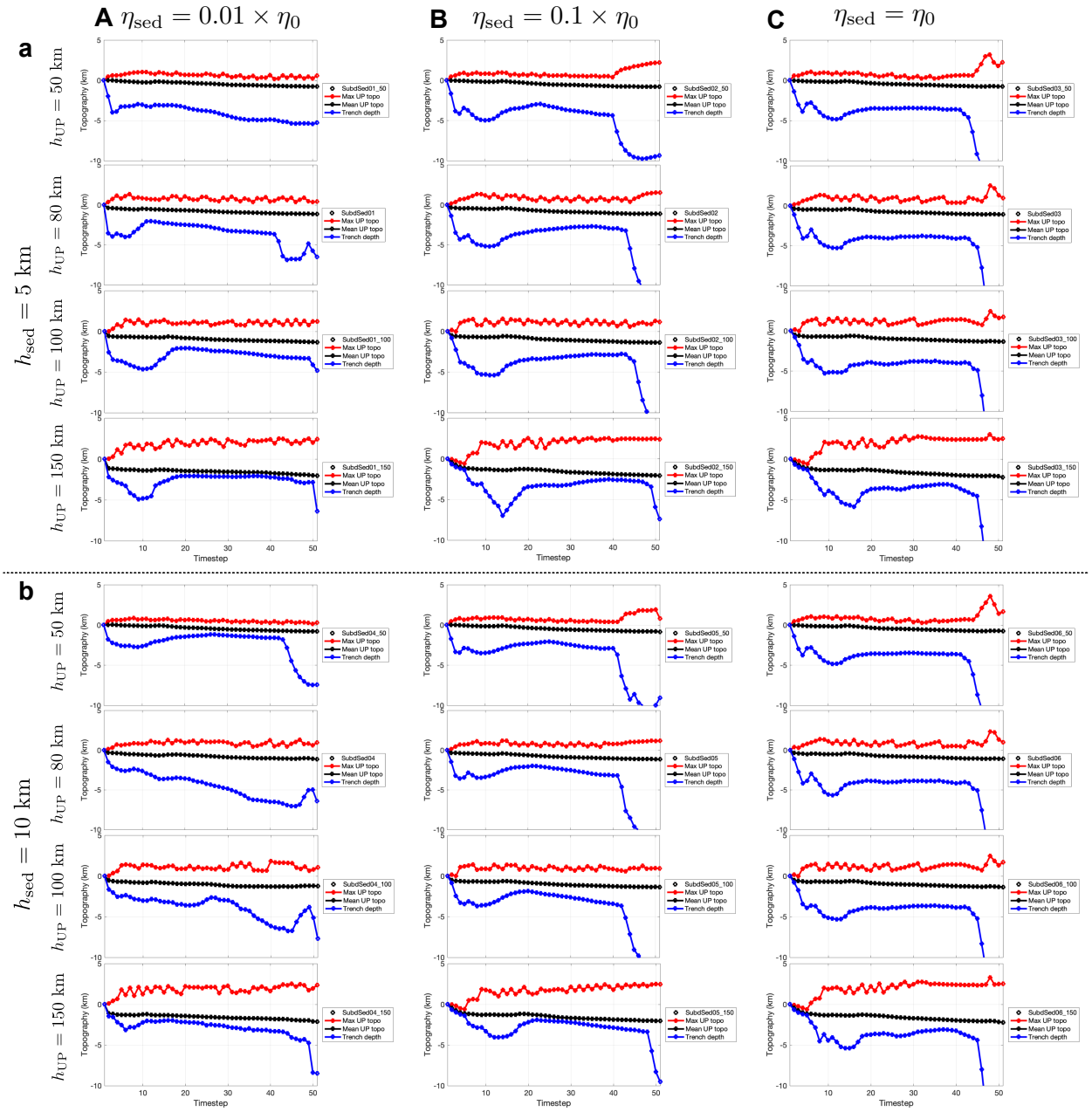

Figure S18. Simulation results - Evolution of topography diagnostics: h_{trench} - trench depth, h_{max} - maximum topographic amplitude in the upper plate, h_{mean} - mean topographic amplitude in the upper plate.